Journal of Inorganic Biochemistry 198 (2019) 110728

Contents lists available at ScienceDirect

Journal of Inorganic Biochemistry

journal homepage: www.elsevier.com/locate/jinorgbio

Flavonol biosynthesis by nonheme iron dioxygenases: A computational study into the structure and mechanism

Neelam Zeb[a,b,c], Muhammad H. Rashid[b,c], M. Qadri E. Mubarak[a], Sidra Ghafoor[a,d], Sam P. de Visser[a,*]

[a] Manchester Institute of Biotechnology and School of Chemical Engineering and Analytical Science, The University of Manchester, 131 Princess Street, Manchester M1 7DN, United Kingdom
[b] National Institute for Biotechnology and Genetic Engineering (NIBGE), Jhang Road, P.O. Box 577, Faisalabad, Pakistan
[c] Pakistan Institute of Engineering and Applied Sciences (PIEAS), Islamabad, Pakistan
[d] Department of Chemistry, Government College University Faisalabad, Jhang Road, 3800 Faisalabad, Pakistan

ARTICLE INFO

Keywords:
Enzyme mechanism
Density functional theory
Cluster model
Nonheme iron
Hydroxylation

ABSTRACT

Plants produce flavonol compounds for vital functions regarding plant growth, fruit and flower colouring as well as fruit ripening processes. Several of these biosynthesis steps are stereo- and regioselective and are being carried out by nonheme iron enzymes. Using density functional theory calculations on a large active site model complex of flavanone-3β-hydroxylase (FHT), we established the mechanism for conversion of naringenin to its dihydroflavonol, which is a key step in the mechanism of flavonol biosynthesis. The reaction starts with dioxygen binding to the iron(II) centre and a reaction with α-ketoglutarate co-substrate gives succinate, an iron(IV)-oxo species and CO_2 with large exothermicity and small reaction barriers. The rate-determining reaction step in the mechanism; however, is hydrogen atom abstraction of an aliphatic C—H bond by the iron(IV)-oxo species. We identify a large kinetic isotope effect for the replacement of the transferring hydrogen atom by deuterium. In a final step the OH and substrate radicals combine to form the alcohol product with a barrier of several kcal mol^{-1}. We show that the latter is the result of geometric constraints in the active site pocket. Furthermore, the calculations show that a weak tertiary C—H bond is shielded from the iron(IV)-oxo species in the substrate binding position and therefore the enzyme is able to activate a stronger C—H bond. As such, the flavanone-3β-hydroxylase enzyme reacts regioselectively with one specific C—H bond of naringenin by avoiding activation of weaker bonds through tight substrate and oxidant positioning.

1. Introduction

Nonheme iron dioxygenases are a versatile class of enzymes in nature that are involved in biosynthesis and biodegradation reactions in almost all forms of life [1–8]. For instance, in the human body, nonheme iron dioxygenases are responsible for the catabolism of cysteine through cysteine dioxygenase [9–11] as well as DNA base repair functions by the AlkB repair enzymes [12–14]. Some of these reactions are stereo- and chemoselective, for instance the biosynthesis of R-hydroxyproline from proline by the nonheme iron dioxygenase prolyl-4-hydroxylase is regio- and stereospecific [15], which has triggered interest of the biotechnology industry into utilizing these enzymes for the stereo- and chemoselective synthesis of products. Understanding the mechanistic and structural features that determine these selectivities is, therefore, important.

In plants nonheme iron dioxygenases take part in the biosynthesis of a series of flavonoids, which are important plant hormones that trigger fruit colouring [16,17], fruit ripening [18] but also operate as stress responses [19,20]. Furthermore, these compounds have been shown to have health benefits in humans and have been correlated to antioxidant and anticancer properties and blood pressure control [21]. Biochemical studies showed that most of these enzymes use iron, moreover, α-ketoglutarate (αKG) is essential for the biosynthesis of most flavonoids in plants [22,23]. Thus, the biosynthesis of flavonols in plants is carried out by a cascade of nonheme iron dioxygenases (Scheme 1), which utilize α-ketoglutarate and dioxygen on an iron centre [24,25] for substrate hydroxylation and desaturation reactions. One particular nonheme iron dioxygenases, namely flavanone-3β-hydroxylase (FHT), converts naringenin into dihydroflavonol on an iron(II) centre [26–29] through aliphatic hydroxylation of the C^3—H bond. Thereafter, another

* Corresponding author.
E-mail address: sam.devisser@manchester.ac.uk (S.P. de Visser).

https://doi.org/10.1016/j.jinorgbio.2019.110728
Received 4 April 2019; Received in revised form 13 May 2019; Accepted 29 May 2019
Available online 04 June 2019

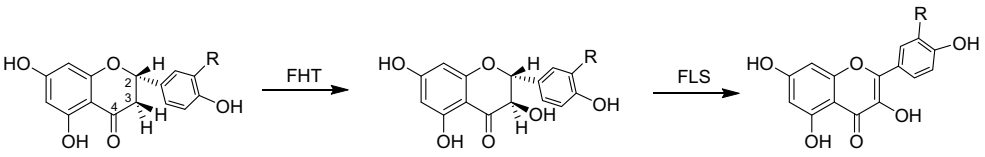

Scheme 1. Conversion of flavanone into flavonol products by nonheme iron dioxygenases FHT and FLS.

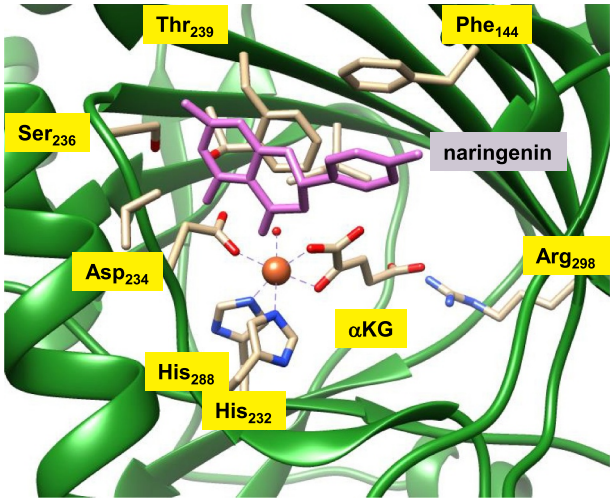

Fig. 1. Active site structure of substrate and αKG-bound FHT as taken from the 2BRT pdb file.

nonheme iron dioxygenase, namely flavonol synthase (FLS) dehydrogenates the C^2–C^3 bond in dihydroflavonol to form flavonol. Little is known on the mechanism of the FHT reaction and the effect of substrate positioning and binding. To gain insight, we explored the mechanism of conversion of naringenin by FHT into dihydroflavonol using computational methods.

Nonheme iron dioxygenases have a well-defined structure [30,31] that has the metal bound through a facial triad with two histidines and one carboxylate ligand in a 2-His/1-Asp or 2-His/1-Glu configuration. As an example, we show the active site structure of FHT as taken from the 2BRT protein databank (pdb) file in Fig. 1 [32]. The metal binds to the side chains of His_{232}, Asp_{234} and His_{288}, which leaves three coordination sites of iron vacant that are filled up by αKG (two sites) and water. The αKG is held in a rigid conformation and binds iron through one carboxylate, whereas the other carboxylate group forms a salt bridge with the Arg_{298} residue. Substrate naringenin binds nearby the metal centre and is locked inside the loop of amino acid residues from Asp_{234} to Thr_{239}, whereas the substrate binding pocket is lined with apolar residues such as Phe_{144}. Apart from π-stacking interactions with aromatic residues the substrate is stabilized with hydrogen bonding interactions of the alcohol groups of Ser_{236} and Thr_{239}.

Early density functional theory calculations on the mechanism of substrate activation by FHT [33] started from another pdb file, namely the IGP6 pdb file, which is an open configuration of the protein without bound substrate and α-ketoglutarate. The authors created a model and inserted trans-dihydroquercetin as a substrate. However, a small truncated cluster model was studied that only contained substrate and the first coordination sphere of metal ligands. Recently [34–36], we showed that substrate binding and positioning in nonheme iron dioxygenases is vital for the reaction mechanism and determines the selectivity and product distributions. As such we decided to revisit the mechanism of naringenin activation by FHT enzymes by an elaborate active site model that includes a large part of the substrate binding pocket and the first- and second-coordination sphere of the iron centre. We show that the protein positions the substrate and oxidant under an ideal conformation for C^3 hydroxylation that is performed by a high-valent iron(IV)-oxo species generated from α-ketoglutarate in a reaction with dioxygen on an iron centre.

2. Methods

We created an active site model based on the crystal structure coordinates deposited as the 2BRT protein databank (pdb) file [32]. This is an flavanone-3β-hydroxylase monomer structure with iron(II), α-ketoglutarate and naringenin bound. Our set-up follows previously described procedures and will be summarized briefly here [37–39]. The structure represents wildtype and has no missing residues in the core region of the protein. We added hydrogen atoms using PropKa [40] based on protonation states of residues at pH = 7, whereby carboxylic acids were deprotonated and Arg and Lys residues protonated. Histidine residues were visually inspected and the three His residues in our model complex (His_{232}, His_{270} and His_{288}) were singly protonated. Finally, the iron(II)-water group was replaced by iron(III)-superoxo to generate the starting point of the catalytic cycle. Solvent (water) was added to the structure and equilibrated. Subsequently, we created an active site model from the fully equilibrated enzyme structure that includes the oxidant and the key parts of the substrate binding pocket as described in Scheme 2. The model included the iron with its first-coordination sphere ligands, i.e. ethylimidazole for His_{232}, methylimidazole for His_{288} and a protein chain connecting Asp_{234} to Thr_{239}. The substrate binding pocket is lined with the peptide chain Asp_{234}-Val_{235}-Ser_{236}-Ala_{237}-Leu_{238}-Thr_{239}, which was kept in the model with the Ala and Leu residues abbreviated to Gly as their side chains point away from the substrate binding pocket. In addition, we included an ethylbenzene moiety representing Phe_{144} and methylguanidine for the Arg_{298} side chain. Overall the model had 170 atoms, was overall charge neutral and was studied with odd spin multiplicity, i.e. singlet, triplet, quintet and

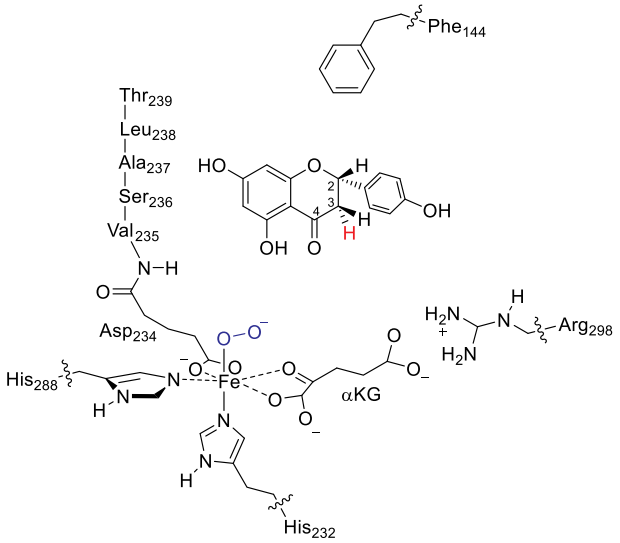

Scheme 2. Active site model of FHT as studied with density functional theory. Wiggly lines identify where the protein chain was cut.

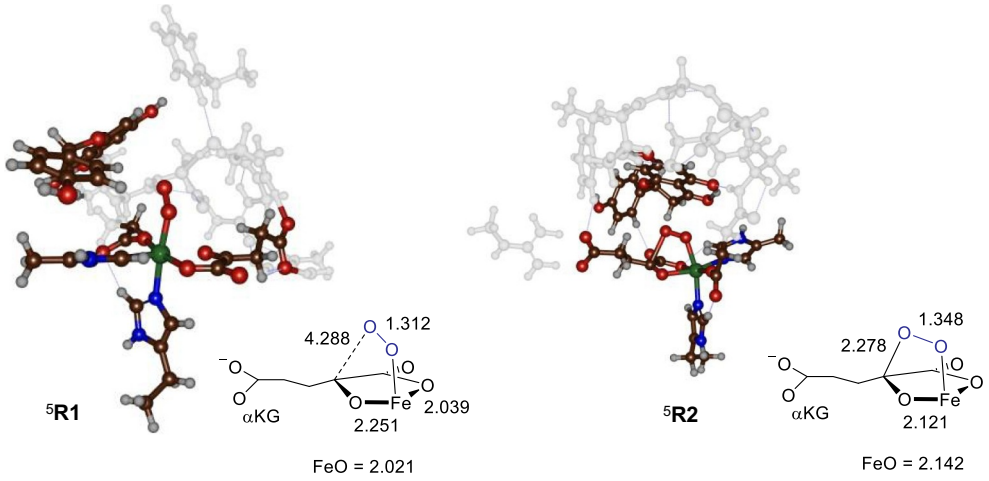

Fig. 2. Optimized geometries of ^{5}R1 and ^{5}R2 of an active site FHT model as calculated with UB3LYP/BS1 in Gaussian-09. Bond lengths are in angstroms.

septet spin. As the residues formed multiple hydrogen bonding interactions, no constraints on the geometry were placed. Recent Quantum Mechanics/Molecular Mechanics and Molecular Dynamics simulations on enzymatic structures of nonheme iron enzymes showed that conformation changes surrounding substrate binding can affect catalysis and selectivity of a reaction [41,42]; hence we optimize our model fully without geometric constraints included to accommodate the system to that flexibility.

Density functional theory (DFT) calculations were performed on the model in Scheme 2 using the Gaussian-09 [43] software package. We utilized the unrestricted hybrid DFT method UB3LYP [44,45] for geometry optimizations, analytical frequencies and geometry scans. Due to the size of the chemical system a modest LACVP basis set on iron with core potential and 6-31G on the rest of the atoms was applied: basis set BS1 [46,47]. To improve the energies single point calculations on the optimized geometries were done with the LACV3P+ basis set on iron with core potential and 6–311 + G* on the rest of the atoms: basis set BS2. Solvent was included with the continuum polarized conductor model (CPCM) [48] with a dielectric constant mimicking chlorobenzene. Dispersion corrections were included with the D3 model of Grimme et al. [49]. These methods and procedures were extensively tested and benchmarked previously and showed to reproduce experimental rate constants within a few kcal mol^{-1} [50–53].

Kinetic isotope effects (KIE) were calculated as before [54,55] using the Eyring (Eq. (1)) and Wigner (Eqs. (2) and (3)) models. We re-evaluated the frequencies and consequently, the entropy and zero-point corrections by replacing the transferring hydrogen atom on C^3 by a deuterium atom to get the primary kinetic isotope effect. In addition, we calculated the secondary kinetic isotope effect by replacing the non-transferring hydrogen atom on C^3 by deuterium. Finally the combined kinetic isotope effect for replacement of both hydrogen atoms attached to C^3 of the substrate by deuterium was investigated. The Eyring KIE is based on the ratio of rate constants of the hydrogen and deuterium containing systems and calculated from the difference in free energy of the hydrogen ($\Delta G^{\ddagger}_H$) and deuterium-substituted ($\Delta G^{\ddagger}_D$) systems with R being the gas constant and T the estimated temperature (298 K). The Wigner kinetic isotope effect is calculated from the Eyring KIE multiplied by the tunnelling ratio estimated from Eq. (3) with h, k_B and T representing Planck's constant, the Boltzmann constant and the temperature, respectively, whereas ν is the imaginary frequency in the transition state.

$$KIE_{Eyring} = \exp\{(\Delta G^{\ddagger}_D - \Delta G^{\ddagger}_H)/RT\} \quad (1)$$

$$KIE_{Wigner} = KIE_{Eyring} \times Q_{t,H}/Q_{t,D} \quad (2)$$

$$Q_t = 1 + (h\nu/k_BT)^2/24 \quad (3)$$

3. Results and discussion

Thanks to a series of detailed spectroscopic [56–58] and computational [59–61] studies, the catalytic cycle of the nonheme iron dioxygenase taurine/α-ketoglutarate dioxygenase (TauD) was established and several short-lived intermediates characterized. These studies revealed that the catalytic cycle of α-ketoglutarate-dependent nonheme iron dioxygenases starts by binding of α-ketoglutarate to the iron(II) centre and is followed by substrate binding in its vicinity. Subsequently, dioxygen binds to iron(II) and forms an iron(III)-superoxo complex (structure **R1**), which initiates the oxygen activation process by attacking the α-keto position of α-ketoglutarate to form a bicyclic ring structure **R2**. Thereafter, the dioxygen bond cleaves to form succinate, CO_2 and an iron(IV)-oxo active species (**R3**). Most of these intermediates are short-lived and only evidence of an iron(IV)-oxo intermediate exists in TauD enzymes [56–58]. It was characterized with resonance Raman, electron paramagnetic resonance and Mössbauer spectroscopy experiments. These studies identified its ground state as a quintet spin state and rate constants of substrate activation implicated a large kinetic isotope effect for replacement of the activated C—H bond with C—D. Hence, hydrogen atom abstraction by the iron(IV)-oxo is expected to be the rate-determining reaction step in TauD. Experimental work on TauD failed to trap and characterize an iron(III)-superoxo species, but recent spectroscopic (UV–Vis, EPR and Mössbauer) studies on cysteine dioxygenase obtained spectra reminiscent of this species [62]. Cysteine dioxygenase; however, does not utilize α-ketoglutarate in its catalytic cycle and transfers two oxygen atoms of O_2 sequentially to the sulfur atom of a cysteinate residue [63,64]. To find out if the catalytic cycle of FHT proceeds via a similar mechanism we set up a model of the active site and calculated the analogous intermediates to those reported for TauD.

As little is known on the catalytic cycle of FHT and no short-lived dioxygen bound intermediates have been trapped and characterized, we decided to start our work with calculations of structures **R1**, **R2** and **R3**. Optimized geometries of **R1**, **R2** and **R3** are given in Figs. 2 and 3. In all cases the quintet spin state is the ground state even though we also calculated the lowest lying singlet, triplet and septet spin states (see Supporting Information) the alternative spin states are well higher in energy. In the iron(III)-superoxo state, the septet spin state is the closest to the quintet ground state by $\Delta E + ZPE = 7.5$ kcal mol^{-1}, while the triplet and singlet spin states are 20.6 and 42.8 kcal mol^{-1} higher lying, respectively. Consequently, the singlet and triplet spin states do not play a role of importance in the oxygen activation process leading up to the iron(IV)-oxo species. Furthermore, even though the septet is close to the quintet spin state in structure **R1**, actually its barrier leading to the

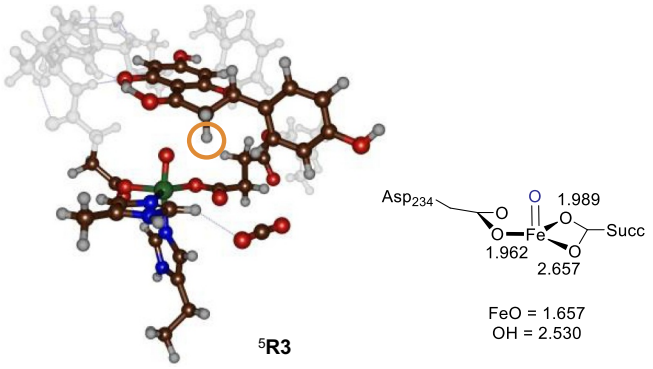

Fig. 3. Optimized geometry of ^{5}R3 of an active site FHT model as calculated with UB3LYP/BS1 in Gaussian-09. Bond lengths are in angstroms. The orange circle indicates the hydrogen atom of the substrate that will be activated next.

ring-structure **R2** is very high and as a result we did not manage to locate a local minimum for ^{7}**R2**. Therefore, the conversion of the iron (III)-superoxo(α-ketoglutarate) structure **R1** into an iron(IV)-oxo(succinate/CO_2) complex takes place through single-state-reactivity on a quintet spin state surface only. Our calculations for this pathway matches previous models of TauD well and follow the same energy landscape [59–61,65].

The quintet spin optimized geometries of **R1** and **R2** are given in Fig. 2 and show the attack of the superoxo moiety on the α-keto-position of α-ketoglutarate. Indeed, the distance between the terminal oxygen atom of the peroxo group and the α-keto carbon atom reduces from 4.288 Å to 2.278 Å between ^{5}**R1** and ^{5}**R2**. At the same time, the O—O bond elongates from 1.312 to 1.348 Å and the Fe—O interaction from 2.021 to 2.142 Å. Energetically, ^{5}**R2** is lesser stable than ^{5}**R1** by $\Delta E + ZPE = 9.6\ kcal\ mol^{-1}$, which matches the values found for small model complexes excellently. Endothermicities of 10.4 kcal mol^{-1} were reported in Ref [59] and 9.6 kcal mol^{-1} in Ref [61]. As such the protein has little effect on the dioxygen activation pathway and the relative energies of the iron(III)-superoxo and ring-structures (**R1** vs **R2**).

Next, we calculated the iron(IV)-oxo species (**R3**) and find it 50.2 kcal mol^{-1} lower in energy than ^{5}**R1**. In agreement with experimental observation on analogous nonheme iron dioxygenases [56–58,66] the quintet spin state is the ground state. The optimized geometry of the iron(IV)-oxo species (^{5}**R3**) of FHT is given in Fig. 3. We also calculated the lowest lying singlet, triplet and septet spin states and find them $\Delta E + ZPE = 32.8$, 3.7 and 7.0 kcal mol^{-1} higher in energy than the quintet spin ground state. The Fe—O bond in ^{5}**R3** is short, i.e. 1.657 Å, which is typical for iron(IV)-oxo bond and matches previous calculations of nonheme iron complexes [59–61,66–75].

The high-lying occupied and low-lying virtual orbitals of the iron (IV)-oxo species are given in Fig. 4. Low in energy are a pair of bonding orbitals (π_{xz} and π_{yz}) between the iron and oxo species that are built up from the $3d_{xz}/3d_{yz}$ on iron with the $2p_x/2p_y$ on oxygen, whereby we take the z-axis along the iron(IV)-oxo bond. Both π_{xz} and π_{yz} are doubly occupied with two electrons. Higher in energy are four singly occupied molecular orbitals that give the iron(IV)-oxo species its quintet spin ground state. Lowest of those are the three π* orbitals; two along the Fe—O bond, namely the π^*_{xz} and π^*_{yz} orbitals, and a third one (π^*_{xy}) in the xy-plane for interactions with, e.g., the carboxylic acid groups of succinate and Asp_{235} and the nitrogen of His_{188}. The fourth singly occupied molecular orbital is the $\sigma^*_{x2\text{-}y2}$ orbital that also is lying in the xy-plane but has its lobes on the x- and y-axis. The σ^*_{z2} orbital for the antibonding interaction of the iron $3d_{z2}$ with the $2p_z$ on oxo and the $2p_z$ on the axial histidine ligand is virtual. Overall this gives the iron(IV)-oxo complex an orbital configuration of $\pi^*_{xy}{}^{1}\ \pi^*_{xz}{}^{1}\ \pi^*_{yz}{}^{1}\ \sigma^*_{x2\text{-}y2}{}^{1}$. In the triplet spin state an orbital occupation of $\pi^*_{xy}{}^{2}\ \pi^*_{xz}{}^{1}\ \pi^*_{yz}{}^{1}\ \sigma^*_{x2\text{-}y2}{}^{0}$ is found and results in promoting the singly occupied electron from $\sigma^*_{x2\text{-}y2}$ into the π^*_{xy} orbital.

At this stage, we reasoned that a comparison of the model with the original crystal structure coordinates would be appropriate. To this end, we compared our optimized geometry of ^{5}**R3** with the crystal structure coordinates of the original 2BRT pdb file and created an overlay of the two structures as given in Fig. 5 with the original pdb structure in green. As can be seen, the peptide chain Asp_{234}-Val_{235}-Ser_{236}-Ala_{237}-Leu_{238} is in virtually the same position with respect to the iron atom in both structures, although some of the side chains have moved slightly with respect to the original pdb. In particular, the Asp carboxylate group is in a slightly lower position in our model due to the fact that both histidine moieties moved sideways. Of course, α-ketoglutarate was replaced by succinate and an oxo group, whereby the oxo group points in the direction of the substrate C^3-position and the carboxylic acid group of succinate is in the plane with the carboxylic acid group of Asp_{234} and the imidazole group of His_{232}. As such, the reaction of O_2 with αKG on an iron(II) centre will generate an iron(IV)-oxo group that is pointing to the C^3-position of substrate and most likely abstract a hydrogen atom there. The structural comparison of the crystal structure coordinates with our optimized geometry shows that the model is a good representation of the actual enzyme and even though no constraints were placed on peptide residues, most of the characteristics of the substrate binding pocket are retained. Interestingly, even though the Phe_{144} residue was abbreviated to ethylbenzene and had no geometric constraints, it actually did not move dramatically in position during the geometry optimizations. This is due to weak hydrogen bonding interactions of its C—H groups with the alcohol group of Thr_{239}, the carboxylic acid group of succinate and the alcohol group of substrate (Supporting Information Fig. S6). Moreover, the position of the oxidant and substrate shows that it is set-up for activation of the C^3—H bond as expected from the product distributions. To test whether there are energetic feasibilities for abstracting hydrogen atoms from the C^3 and C^2 positions, we followed the work up with a DFT study of substrate hydroxylation by the iron(IV)-oxo species from these positions.

To complete the catalytic cycle, we calculated the substrate hydroxylation at the C^3-position of naringenin by the iron(IV)-oxo species. The reaction is stepwise via a hydrogen atom abstraction transition state ($\mathbf{TS}_{HA}$) that leads to an iron(III)-hydroxo and radical intermediate (**IM1**). Thereafter, the OH and radical couple via a rebound transition state ($\mathbf{TS}_{reb}$) to form the dehydroflavonol product (**Pr**). The mechanism as calculated on the quintet and triplet spin states are given in Fig. 6. As can be seen the quintet spin state is the lowest energy state and stays the ground state along the full reaction profile. The hydrogen atom abstraction barrier is calculated to be $\Delta E + ZPE = 8.4\ kcal\ mol^{-1}$ from the iron(IV)-oxo intermediate, whereas the rebound is $\Delta E + ZPE = 4.9\ kcal\ mol^{-1}$ above ^{5}**IM1**. These barriers are typical for aliphatic hydrogen atom abstraction of secondary C—H atoms by iron (IV)-oxo complexes [76–80]. The $^{5}\mathbf{TS}_{HA}$ structure is product-like with a short O—H distance of 1.183 Å, while the C—H distance is much longer at 1.332 Å. It has a large imaginary frequency of $i1492cm^{-1}$, which is typical for hydrogen atom abstraction transition states [81–83]. The triplet spin barrier is well higher in energy (by > 20 kcal mol^{-1}) and has a long C—H bond of 1.486 Å. The hydrogen atom abstraction in the quintet spin state results in electron transfer into the virtual σ^*_{z2} orbital and generates a radical intermediate with $\pi^*_{xy}{}^{1}\ \pi^*_{xz}{}^{1}\ \pi^*_{yz}{}^{1}\ \sigma^*_{x2\text{-}y2}{}^{1}\ \sigma^*_{z2}{}^{1}\ \sigma_{Sub}{}^{1}$ configuration with the metal 3d-block orbitals with up-spin and the σ_{Sub} electron as down-spin. Indeed, the group spin densities give a value of −1.0 on the substrate and 4.2 on the metal, while the rest is distributed over the direct ligands of the metal.

We also tested hydrogen atom abstraction of the other C^3—H group of naringenin by the iron(IV)-oxo species, but due to stereochemical constraints on substrate binding and orientation this is not a feasible pathway. A constraint geometry scan for the O—H approach was performed and the energy continuously increases with respect to that of the iron(IV)-oxo species and does not reach a stable radical intermediate. As such, the positioning of substrate limits the possibility of

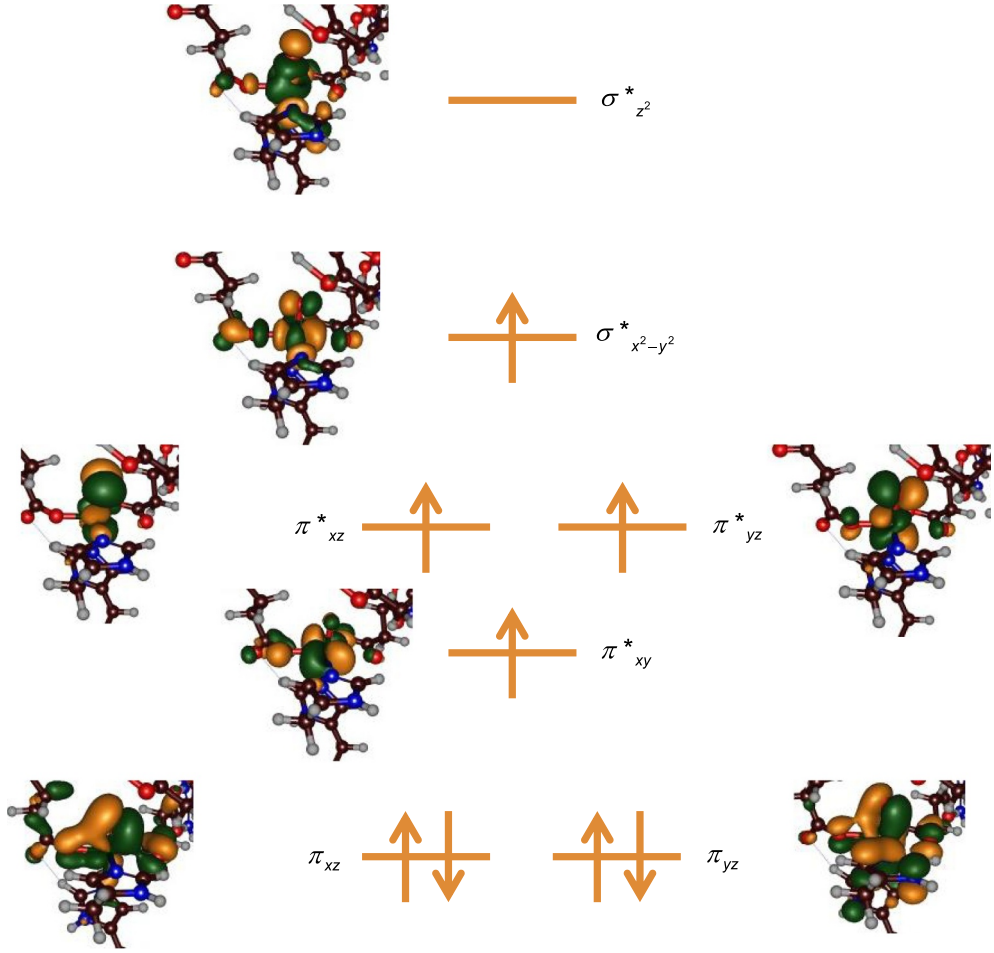

Fig. 4. Orbital energy levels of ^{5}R3 as calculated at UB3LYP/BS1 in Gaussian.

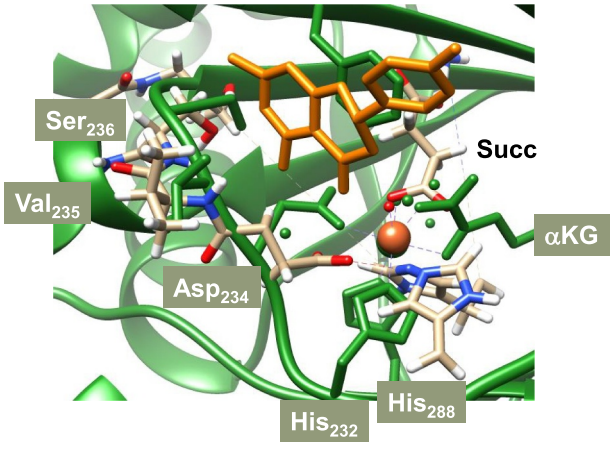

Fig. 5. Overlay of the optimized UB3LYP/BS1 geometry of ^{5}R3 with the crystal structure coordinates of 2BRT (in green).

the iron(IV)-oxo species to abstract hydrogen atoms from the substrate and only one hydrogen atom of the C^3—H group can be selectively abstracted.

Interestingly, the rebound barrier in the mechanism of naringenin activation by FHT is relatively high in energy, i.e. 4.9 kcal mol^{-1} above ^{5}**IM1**. However, the hydrogen atom abstraction is still the rate-determining step in the catalytic cycle. The origin of the relatively high rebound barrier is probably because of a tight substrate bound orientation in the active site. Indeed, in analogous nonheme iron enzymes with tight substrate-bound pocket often the rebound barrier is high in energy due to geometric constraints [34–38,84,85]. However, we do not expect that the radical will leave the substrate binding pocket as it is bound by a number of hydrogen bonding interactions and it will; therefore, require a substantial amount of energy to break these bonds.

Overall, the rate-determining step for the reaction of the iron(IV)-oxo species with substrate is the hydrogen atom abstraction via ^{5}**TS**$_{HA}$, hence it will be affected by isotopic substitution leading to a kinetic isotope effect. Thus, we re-evaluated the free energies of activation by replacing the transferring hydrogen atom by deuterium as well as replacing the other hydrogen atom bound to C^3 by deuterium, see Table 1. As can be seen the secondary KIE is very small (KIE_{Eyring} = 1.08), which means that only the transferring hydrogen atom contributes to the isotope effect. The primary isotope effect is in the range of the typical isotope effects seen for nonheme iron enzymes and biomimetic model complexes [68,86] with values of KIE_{Eyring} = 7.73 and KIE_{Wigner} = 10.85. These KIEs imply a significant amount of quantum mechanical tunnelling and considerably faster rates for hydrogen than deuterium.

Finally, constraint geometry scans for C^2—H hydrogen atom abstraction and ortho-phenol hydroxylation were performed but due to geometric constraints on substrate positioning and the shape and size of the substrate binding pocket, neither of these pathways were found to be energetically feasible.

In summary, we find a stepwise substrate hydroxylation mechanism on a low-lying quintet spin state surface. Alternative spin states were calculated but found to be considerably higher in energy and will not play a role of importance. As such flavanone-3β-hydroxylase reacts via single-state reactivity on a dominant quintet spin-state surface. The

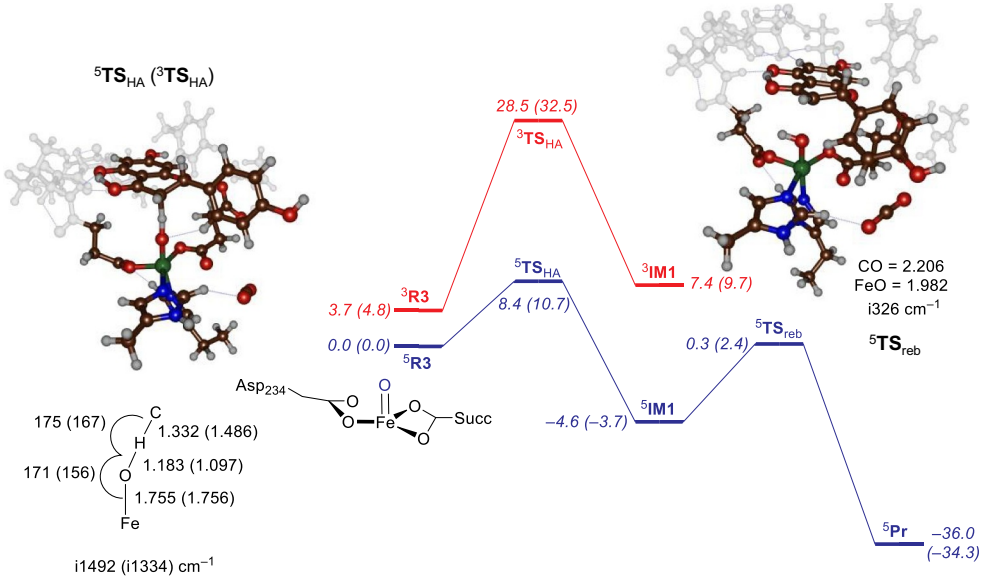

Fig. 6. Potential energy landscape for substrate hydroxylation by an iron(IV)-oxo species using a model of the active site FHT. Structures optimized at UB3LYP/BS1 in Gaussian-09 and (free) energies are given at UB3LYP/BS2 with solvent, thermal and zero-point corrections in kcal mol^{-1}. Bond lengths of optimized geometries are in angstroms and angles in degrees. The imaginary frequency in the transition state is given in cm^{-1}.

Table 1
Calculated KIE effects on $^5TS_{HA}$ using the Eyring and Wigner models.

	D_aH_b[a]	H_aD_b[a]	D_aD_b[a]
KIE_{Eyring}[b]	7.73	1.08	8.49
KIE_{Wigner}[c]	10.85	1.09	12.01

[a] For FeO—H_a–C^3H_bR substitution of hydrogen by deuterium: subscript a refers to the transferring atom and subscript b to the non-transferring atom on position C^3 of the substrate.
[b] Calculated using Eq. (1).
[c] Calculated using Eq. (2).

rate-determining step; however, is the initial hydrogen atom abstraction from the C^3—H position of substrate that is relatively low in energy and hence should proceed fast. Alternative hydrogen atom abstraction channels were also tested. In particular, we tested abstraction of the tertiary C—H atom at the C^2 position of substrate as well as the other hydrogen atom at the C^3 position. However, due to their positioning these hydrogen atom abstraction processes require a major reorientation of the substrate, which led to high energy pathways. Therefore, the selectivity of this protein is thanks to substrate binding and positioning in the substrate binding pocket.

4. Conclusions

In this work a cluster model study on the enzyme flavanone-3β-hydroxylase is reported and the hydroxylation of naringenin explored. We find a stepwise reaction mechanisms where dioxygen binding gives an iron(III)-superoxo species that is converted into an iron(IV)-oxo through activation of α-ketoglutarate. This process takes place on a quintet spin ground state and is followed by a hydrogen atom abstraction and OH rebound process to form hydroxylated product. The work shows that ideal substrate and oxidant positioning is required to give efficient substrate hydroxylation.

Acknowledgements

NZ thanks the Higher Education Commission of Pakistan for a travel bursary and the National Institute for Biotechnology and Genetic Engineering (NIBGE) in Faisalabad (Pakistan) for a studentship. MQEM acknowledges the Government of Malaysia for a studentship. SH thanks the Higher Education Commission of Pakistan for a travel grant.

Appendix A. Supplementary data

Supplementary data to this article can be found online at https://doi.org/10.1016/j.jinorgbio.2019.110728.

References

[1] E.I. Solomon, T.C. Brunold, M.I. Davis, J.N. Kemsley, S.-K. Lee, N. Lehnert, F. Neese, A.J. Skulan, Y.-S. Yang, J. Zhou, Chem. Rev. 100 (2000) 235–349, https://doi.org/10.1021/cr9900275.
[2] T.D.H. Bugg, Curr. Opin. Chem. Biol. 5 (2001) 550–555.
[3] M.J. Ryle, R.P. Hausinger, Curr. Opin. Chem. Biol. 6 (2002) 193–201.
[4] M. Costas, M.P. Mehn, M.P. Jensen, L. Que Jr., Chem. Rev. 104 (2004) 939–986, https://doi.org/10.1021/cr020628n.
[5] P.C.A. Bruijnincx, G. van Koten, R.J.M. Klein Gebbink, Chem. Soc. Rev. 37 (2008) 2716–2744, https://doi.org/10.1039/b707179p.
[6] S.P. de Visser, D. Kumar (Eds.), Iron-Containing Enzymes: Versatile Catalysts of Hydroxylation Reaction in Nature, RSC Publishing, Cambridge (UK), 2011.
[7] R. P. Hausinger, Biochemical diversity of 2-oxoglutarate-dependent oxygenases. In RSC Metallobiology Series No. 3, R. P. Hausinger, C. J. Schofield (Eds.), (Chapter 1), pp 1–58.
[8] S.-S. Gao, N. Naowarojna, R. Cheng, X. Liu, P. Liu, Nat. Prod. Rep. 35 (2018) 792–837, https://doi.org/10.1039/c7np00067g.
[9] M.H. Stipanuk, Annu. Rev. Nutr. 24 (2004) 539–577, https://doi.org/10.1146/annurev.nutr.24.012003.132418.
[10] C.A. Joseph, M.J. Maroney, Chem. Commun. (2007) 3338–3349, https://doi.org/10.1039/b702158e.
[11] D. Buongiorno, G.D. Straganz, Coord. Chem. Rev. 257 (2013) 541–563, https://doi.org/10.1016/j.ccr.2012.04.028.
[12] S.C. Trewick, T.F. Henshaw, R.P. Hausinger, T. Lindahl, B. Sedgwick, Nature 419 (2002) 174–178, https://doi.org/10.1038/nature00908.
[13] P.J. O'Brien, Chem. Rev. 106 (2006) 720–752, https://doi.org/10.1021/cr040481v.
[14] C. Yi, C.G. Yang, C. He, Acc. Chem. Res. 42 (2009) 519–529, https://doi.org/10.1021/ar800178j.
[15] C.J. Schofield, Z. Zhang, Curr. Opin. Struct. Biol. 9 (1999) 722–731.
[16] C. Honda, N. Kotoda, M. Wada, S. Kondo, S. Kobayashi, J. Soejima, Z. Zhang, T. Tsuda, T. Moriguchi, Plant Physiol. Biochem. 40 (2002) 955–962.
[17] S. Martens, A. Preuß, U. Matern, Phytochemistry 71 (2010) 1040–1049, https://doi.org/10.1016/j.phytochem.2010.04.016.
[18] J. Songa, L. Du, L. Li, W. Kalt, L. Campbell Palmer, S. Fillmore, Y. Zhang, Z.Q. Zhang, X.H. Li, J. Proteome 122 (2015) 1–10, https://doi.org/10.1016/j.jprot.2015.03.017.
[19] M. Liu, X. Li, Y. Liu, B. Cao, Plant Physiol. Biochem. 73 (2013) 161–167, https://doi.org/10.1016/j.plaphy.2013.09.016.
[20] C. Li, S. Liu, X. Yao, J. Wang, T. Wang, Z. Zhang, P. Zhang, K. Chen, Plant Growth Regul. 83 (2017) 489–500, https://doi.org/10.1007/s10725-017-0314-z.
[21] T. Tohge, M. Watanabe, R. Hoefgen, A.R. Fernie, Crit. Rev. Biochem. Mol. Biol. 48 (2013) 123–152, https://doi.org/10.3109/10409238.2012.758083.
[22] E. Soubeyrand, S. Colombié, B. Beauvoit, Z. Dai, S. Cluzet, G. Hilbert, C. Renaud, L. Maneta-Peyret, M. Dieuaide-Noubhani, J.-M. Mérillon, Y. Gibon, S. Delrot, E. Gomès, Front. Plant Sci. 9 (2018) 421, , https://doi.org/10.3389/fpls.2018.00421.
[23] M.D. White, E. Flashman, Curr. Opin. Chem. Biol. 31 (2016) 126–135, https://doi.org/10.1016/j.cbpa.2016.02.017.

[24] A.-X. Cheng, X.-J. Han, Y.-F. Wu, H.-X. Lou, Int. J. Mol. Sci. 15 (2014) 1080–1095, https://doi.org/10.3390/ijms15011080.
[25] J.J. Turnbull, J.-i. Nakajima, R.W.D. Welford, M. Yamazaki, K. Saito, C.J. Schofield, J. Biol. Chem. 279 (2004) 1206–1216, https://doi.org/10.1074/jbc.M309228200.
[26] F. Jiang, J.-Y. Wang, H.-F. Jia, W.-S. Jia, H.-Q. Wang, M. Xiao, J. Plant Growth Regul. 32 (2013) 182–190, https://doi.org/10.1007/s00344-012-9289-1.
[27] R. Lukačin, I. Gröning, E. Schiltz, L. Britsch, U. Matern, Arch. Biochem. Biophys. 375 (2000) 364–370, https://doi.org/10.1006/abbi.1999.1676.
[28] H. Halbwirth, T.C. Fischer, K. Schlangen, W. Rademacher, K.-J. Schleifer, G. Forkmann, K. Stich, Plant Sci. 171 (2006) 194–205, https://doi.org/10.1016/j.plantsci.2006.03.014.
[29] D.K. Owens, K.C. Crosby, J. Runac, B.A. Howard, B.S.J. Winkel, Plant Physiol. Biochem. 46 (2008) 833–843, https://doi.org/10.1016/j.plaphy.2008.06.004.
[30] V. Purpero, G.R. Moran, J. Biol. Inorg. Chem. 12 (2007) 587–601, https://doi.org/10.1007/s00775-007-0231-0.
[31] W. S. Aik, R. Chowdhury, I. J. Clifton, R. J. Hopkinson, T. Leissing, M. A. McDonough, R. Nowak, C. J. Schofield, L. J. Walport, Introduction to structural studies on 2-oxoglutarate-dependent oxygenases and related enzymes, In RSC Metallobiology Series No. 3, R. P. Hausinger, C. J. Schofield (Eds.), (Chapter 2), pp 59–94.
[32] R.W.D. Welford, I.J. Clifton, J.J. Turnbull, S.C. Wilson, C.J. Schofield, Org. Biomol. Chem. 3 (2005) 3117–3126, https://doi.org/10.1039/b507153d.
[33] J.-i. Nakajima, Y. Sato, T. Hoshino, M. Yamazaki, K. Saito, J. Biol. Chem. 281 (2006) 21387–21398, https://doi.org/10.1074/jbc.M600303200.
[34] A. Timmins, M. Saint-André, S.P. de Visser, J. Am. Chem. Soc. 139 (2017) 9855–9866, https://doi.org/10.1021/jacs.7b02839.
[35] A. Timmins, N.J. Fowler, J. Warwicker, G.D. Straganz, S.P. de Visser, Front. Chem. 6 (2018) 513, https://doi.org/10.3389/fchem.2018.00513.
[36] S.M. Pratter, C. Konstantinovics, C.L.M. DiGiuro, E. Leitner, D. Kumar, S.P. de Visser, G. Grogan, G.D. Straganz, Angew. Chem. Int. Ed. 52 (2013) 9677–9681 (Angew. Chem. 125 (2013) 9859–9863), https://doi.org/10.1002/anie.201304633.
[37] M.G. Quesne, T. Borowski, S.P. de Visser, Chem. Eur. J. 22 (2016) 2562–2581, https://doi.org/10.1002/chem.201503802.
[38] A.S. Faponle, M.G. Quesne, S.P. de Visser, Chem. Eur. J. 22 (2016) 5478–5483, https://doi.org/10.1002/chem.201600739.
[39] M.G. Quesne, R. Latifi, L.E. Gonzalez-Ovalle, D. Kumar, S.P. de Visser, Chem. Eur. J. 20 (2014) 435–446, https://doi.org/10.1002/chem.201303282.
[40] T.J. Dolinsky, J.E. Nielsen, J.A. McCammon, N.A. Baker, Nucleic Acids Res. 32 (2004) W665–W667.
[41] S.S. Chaturvedi, R. Ramanan, S.O. Waheed, J. Ainsley, M. Evison, J.M. Ames, C.J. Schofield, T.G. Karabencheva-Christova, C.Z. Christov, Chem. Eur. J. 25 (2019) 5422–5426, https://doi.org/10.1002/chem.201900492.
[42] S.O. Waheed, R. Ramanan, S.S. Chaturvedi, J. Ainsley, M. Evison, J.M. Ames, C.J. Schofield, C.Z. Christov, T.G. Karabencheva-Christova, Org. Biomol. Chem. 17 (2019) 2223–2231, https://doi.org/10.1039/c9ob00162j.
[43] M.J. Frisch, G.W. Trucks, H.B. Schlegel, G.E. Scuseria, M.A. Robb, J.R. Cheeseman, G. Scalmani, V. Barone, B. Mennucci, G.A. Petersson, H. Nakatsuji, M. Caricato, X. Li, H.P. Hratchian, A.F. Izmaylov, J. Bloino, G. Zheng, J.L. Sonnenberg, M. Hada, M. Ehara, K. Toyota, R. Fukuda, J. Hasegawa, M. Ishida, T. Nakajima, Y. Honda, O. Kitao, H. Nakai, T. Vreven, J.A. Montgomery Jr., J.E. Peralta, F. Ogliaro, M. Bearpark, J.J. Heyd, E. Brothers, K.N. Kudin, V.N. Staroverov, R. Kobayashi, J. Normand, K. Raghavachari, A. Rendell, J.C. Burant, S.S. Iyengar, J. Tomasi, M. Cossi, N. Rega, J.M. Millam, M. Klene, J.E. Knox, J.B. Cross, V. Bakken, C. Adamo, J. Jaramillo, R. Gomperts, R.E. Stratmann, O. Yazyev, A.J. Austin, R. Cammi, C. Pomelli, J.W. Ochterski, R.L. Martin, K. Morokuma, V.G. Zakrzewski, G.A. Voth, P. Salvador, J.J. Dannenberg, S. Dapprich, A.D. Daniels, Ö. Farkas, J.B. Foresman, J.V. Ortiz, J. Cioslowski, D.J. Fox, Gaussian 09, Revision D.01, Gaussian, Inc., C. T. Wallingford, 2009.
[44] A.D. Becke, J. Chem. Phys. 98 (1993) 5648–5652, https://doi.org/10.1063/1.464913.
[45] C. Lee, W. Yang, R.G. Parr, Phys. Rev. B 37 (1988) 785–789, https://doi.org/10.1103/PhysRevB.37.785.
[46] P.J. Hay, W.R. Wadt, J. Chem. Phys. 82 (1985) 270–283, https://doi.org/10.1063/1.448799.
[47] W.J. Hehre, R. Ditchfield, J.A. Pople, J. Chem. Phys. 56 (1972) 2257–2262, https://doi.org/10.1063/1.1677527.
[48] J. Tomasi, B. Mennucci, R. Cammi, Chem. Rev. 105 (2005) 2999–3093, https://doi.org/10.1021/cr9904009.
[49] S. Grimme, J. Antony, S. Ehrlich, H. Krieg, J. Chem. Phys. 132 (2010) 154104, , https://doi.org/10.1063/1.3382344.
[50] S. Kumar, A.S. Faponle, P. Barman, A.K. Vardhaman, C.V. Sastri, D. Kumar, S.P. de Visser, J. Am. Chem. Soc. 136 (2014) 17102–17115, https://doi.org/10.1021/ja508403w.
[51] M.A. Sainna, S. Kumar, D. Kumar, S. Fornarini, M.E. Crestoni, S.P. de Visser, Chem. Sci. 6 (2015) 1516–1529, https://doi.org/10.1039/c4sc02717e.
[52] F.G. Cantú Reinhard, A.S. Faponle, S.P. de Visser, J. Phys. Chem. A 120 (2016) 9805–9814, https://doi.org/10.1021/acs.jpca.6b09765.
[53] T. Yang, M.G. Quesne, H.M. Neu, F.G. Cantú Reinhard, D.P. Goldberg, S.P. de Visser, J. Am. Chem. Soc. 138 (2016) 12375–12386, https://doi.org/10.1021/jacs.6b05027.
[54] X.-X. Li, V. Postils, W. Sun, A.S. Faponle, M. Solà, Y. Wang, W. Nam, S.P. de Visser, Chem. Eur. J. 23 (2017) 6406–6418, https://doi.org/10.1002/chem.201700363.
[55] F.G. Cantú Reinhard, P. Barman, G. Mukherjee, J. Kumar, D. Kumar, D. Kumar, C.V. Sastri, S.P. de Visser, J. Am. Chem. Soc. 139 (2017) 18328–18338, https://doi.org/10.1021/jacs.7b10033.
[56] J.C. Price, E.W. Barr, B. Tirupati, J.M. Bollinger Jr., C. Krebs, Biochemistry 42 (2003) 7497–7508, https://doi.org/10.1021/bi030011f.
[57] D.A. Proshlyakov, T.F. Henshaw, G.R. Monterosso, M.J. Ryle, R.P. Hausinger, J. Am. Chem. Soc. 126 (2004) 1022–1023, https://doi.org/10.1021/ja039113j.
[58] J.M. Bollinger Jr., J.C. Price, L.M. Hoffart, E.W. Barr, C. Krebs, Eur. J. Inorg. Chem. (2005) 4245–4254, https://doi.org/10.1002/ejic.200500476.
[59] T. Borowski, A. Bassan, P.E.M. Siegbahn, Chem. Eur. J. 10 (2004) 1031–1041, https://doi.org/10.1002/chem.200305306.
[60] A.V. Nemukhin, B.L. Grigorenko, I.A. Topol, S.K. Burt, Int. J. Quantum Chem. 106 (2006) 2184–2190, https://doi.org/10.1002/qua.20910.
[61] S.P. de Visser, Chem. Commun. (2007) 171–173, https://doi.org/10.1039/b611273k.
[62] E.P. Tchesnokov, A.S. Faponle, C.G. Davies, M.G. Quesne, R. Turner, M. Fellner, R.J. Souness, S.M. Wilbanks, S.P. de Visser, G.N.L. Jameson, Chem. Commun. 52 (2016) 8814–8817, https://doi.org/10.1039/c6cc03904a.
[63] D. Kumar, W. Thiel, S.P. de Visser, J. Am. Chem. Soc. 133 (2011) 3869–3882, https://doi.org/10.1021/ja107514f.
[64] A.S. Faponle, F.P. Seebeck, S.P. de Visser, J. Am. Chem. Soc. 139 (2017) 9259–9270, https://doi.org/10.1021/jacs.7b04251.
[65] S.P. de Visser, Chem. Rec. 18 (2018) 1501–1516, https://doi.org/10.1002/tcr.201800033.
[66] S. Sinnecker, N. Svensen, E.W. Barr, S. Ye, J.M. Bollinger Jr., F. Neese, C. Krebs, J. Am. Chem. Soc. 129 (2007) 6168–6179, https://doi.org/10.1021/ja067899q.
[67] S.P. de Visser, J. Am. Chem. Soc. 128 (2006) 9813–9824, https://doi.org/10.1021/ja061581g.
[68] F.G. Cantú Reinhard, S.P. de Visser, Chem. Eur. J. 23 (2017) 2935–2944, https://doi.org/10.1002/chem.201605505.
[69] L. Hu, H. Chen, J. Am. Chem. Soc. 139 (2017) 15564–15567, https://doi.org/10.1021/jacs.7b06086.
[70] I. Prat, A. Company, V. Postils, X. Ribas, L. Que Jr., J.M. Luis, M. Costas, Chem. Eur. J. 19 (2013) 6724–6738, https://doi.org/10.1002/chem.201300110.
[71] H. Hirao, F. Li, L. Que Jr., K. Morokuma, Inorg. Chem. 50 (2011) 6637–6648, https://doi.org/10.1021/ic200522r.
[72] A. Ansari, A. Kaushik, G. Rajaraman, J. Am. Chem. Soc. 135 (2013) 4235–4249, https://doi.org/10.1021/ja307077f.
[73] B. Mondal, F. Neese, E. Bill, S. Ye, J. Am. Chem. Soc. 140 (2018) 9531–9544, https://doi.org/10.1021/jacs.8b04275.
[74] S.P. de Visser, Angew. Chem. Int. Ed. 45 (2006) 1790–1793, Angew. Chem. 118 (2006) 1822–1825, https://doi.org/10.1002/anie.200503841.
[75] E. Godfrey, C.S. Porro, S.P. de Visser, J. Phys. Chem. A 112 (2008) 2464–2468, https://doi.org/10.1021/jp710999v.
[76] S. Shaik, D. Kumar, S.P. de Visser, J. Am. Chem. Soc. 130 (2008) 10128–10140, https://doi.org/10.1021/ja8019615.
[77] R. Latifi, M. Bagherzadeh, S.P. de Visser, Chem. Eur. J. 15 (2009) 6651–6662, https://doi.org/10.1002/chem.200900211.
[78] A. Timmins, M.G. Quesne, T. Borowski, S.P. de Visser, ACS Catal. 8 (2018) 8685–8698, https://doi.org/10.1021/acscatal.8b01673.
[79] A. Takahashi, D. Yamaki, K. Ikemura, T. Kurahashi, T. Ogura, M. Hada, H. Fujii, Inorg. Chem. 51 (2012) 7296–7305, https://doi.org/10.1021/ic3006597.
[80] Y. Wang, Y. Wang, K. Han, J. Biol. Inorg. Chem. 14 (2009) 533–545, https://doi.org/10.1007/s00775-009-0468-x.
[81] S.P. de Visser, D. Kumar, S. Cohen, R. Shacham, S. Shaik, J. Am. Chem. Soc. 126 (2004) 8362–8363, https://doi.org/10.1021/ja048528h.
[82] S.P. de Visser, Chem. Eur. J. 12 (2006) 8168–8177, https://doi.org/10.1002/chem.200600376.
[83] B. Karamzadeh, D. Kumar, G.N. Sastry, S.P. de Visser, J. Phys. Chem. A 114 (2010) 13234–13243, https://doi.org/10.1021/jp1089855.
[84] A. Timmins, S.P. de Visser, Front. Chem. 5 (2017) 94, https://doi.org/10.3389/fchem.2017.00094.
[85] M. Pickl, S. Kurakin, F.G. Cantú Reinhard, P. Schmid, A. Pöcheim, C.K. Winkler, W. Kroutil, S.P. de Visser, K. Faber, ACS Catal. 9 (2019) 565–577, https://doi.org/10.1021/acscatal.8b03733.
[86] P. Barman, P. Upadhyay, A.S. Faponle, J. Kumar, S.S. Nag, D. Kumar, C.V. Sastri, S.P. de Visser, Angew. Chem. Int. Ed. 55 (2016) 11091–11095, https://doi.org/10.1002/anie.201604412.